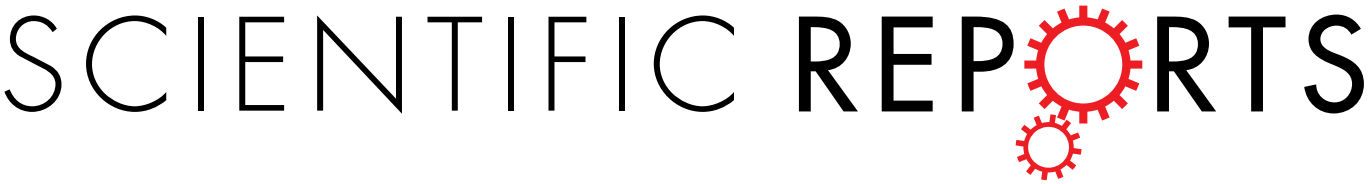

OPEN

Distinct doping dependence of critical temperature and critical current density in $Ba_{1-x}K_xFe_2As_2$ superconductor

Received: 21 September 2015
Accepted: 05 May 2016
Published: 25 May 2016

Dongjoon Song[1], Shigeyuki Ishida[1], Akira Iyo[1], Masamichi Nakajima[2], Jun-ichi Shimoyama[3], Michael Eisterer[4] & Hiroshi Eisaki[1]

Since the high transition temperature (High-T_c) superconductivity was discovered in the series of materials containing iron (Fe), their potential for the applications has been extensively scrutinized. In particular, a lot of effort has been made in achieving the high current-carrying ability by revealing the vortex pinning behavior. Here, we report on the critical current density (J_c) for the pristine $Ba_{1-x}K_xFe_2As_2$ single crystals with various K concentrations ($0.25 \leq x \leq 0.52$) determined by the magnetization hysteresis loop measurements. The x-dependence of J_c is characterized by a spike-like peak at $x \sim 0.30$, which corresponds to the under-doped region. This behavior is distinct from a moderate T_c dome with a broad maximum spanning from $x \sim 0.3$ to 0.5. For the under-doped samples, with increasing magnetic field (H), a second magnetization peak in J_c is observed, whereas for the optimally- and over-doped samples, J_c monotonically decreases with H. This result emphasizes that fine tuning of doping composition is important to obtain strong flux pinning. The origin of the characteristic doping dependence of J_c is discussed in connection with the orthorhombic phase domain boundary, as well as the chemical inhomogeneity introduced by the dopant substitutions.

A high superconducting transition temperature (T_c), upper critical field (H_{c2}), and critical current density (J_c) are the three major requirements for large current and/or high magnetic field applications of superconductivity. Iron (Fe)-based superconductors discovered in 2008[1] are considered to satisfy these requirements because of their relatively high T_c reaching 56 K at highest[2], as well as their high H_{c2} exceeding 100 T[3,4]. In particular, materials derived from $AEFe_2As_2$ (AE = alkaline earth elements), so-called 122 – type materials, were regarded as the most promising candidates, since they possess further attractive properties, such as the small anisotropy factor ($H_{c2}^{//ab}/H_{c2}^{//c} = \gamma = 1 \sim 2$)[5,6], superior inter-grain connectivity[7,8], and easiness in the sample synthesis *etc.* Various thin-films and bulk wires have been fabricated (mostly by powder-in-tube (PIT) methods) using 122-based materials[9,10]. To date, J_c values reach up to 10^6 A/cm^2 for a $BaFe_2(As_{1-x}P_x)_2$ thin film (4 K, 9 T)[11] and 10^5 A/cm^2 for a $Ba_{1-x}K_xFe_2As_2$ (or $Sr_{1-x}K_xFe_2As_2$) PIT wire (4.2 K, 10 T)[12,13], respectively.

While T_c and H_{c2} are intrinsic material parameters and thus more or less determined by the microscopic superconducting mechanism, J_c is effectively determined by vortex pinning in single crystals or films, which is either of intrinsic or extrinsic origin. In general, the pinning force is not strong in homogeneous high-quality single crystals without defects, while introduction of artificial disorder results in enhancement of J_c. From the same point of view, in the case of Fe-based superconductors, many efforts have been paid to develop suitable materials with defect structures which give rise to strong vortex pinning, as well as to understand the fundamental pinning mechanism. As for the former, the introduction of columnar defects by irradiation with high energy particles[14–16] or self-assembling $BaFeO_2$ nanorods[17,18] has been proven to be effective in increasing J_c. As for the latter, it is recognized that the Fe-based superconductors exhibit a second magnetization peak (SMP) in J_c[19–25], which is

[1]Electronics and Photonics Research Institute, National Institute of Advanced Industrial Science and Technology (AIST), Tsukuba 305-8568, Japan. [2]Department of Physics, Osaka University, Toyonaka, Osaka 560-0043, Japan. [3]Department of Physics and Mathematics, Aoyama Gakuin University, Sagamihara 252-5258, Japan. [4]Atominstitut, Vienna University of Technology, Stadionallee 2, 1020 Vienna, Austria. Correspondence and requests for materials should be addressed to D.S. (email: dj-son@aist.go.jp)

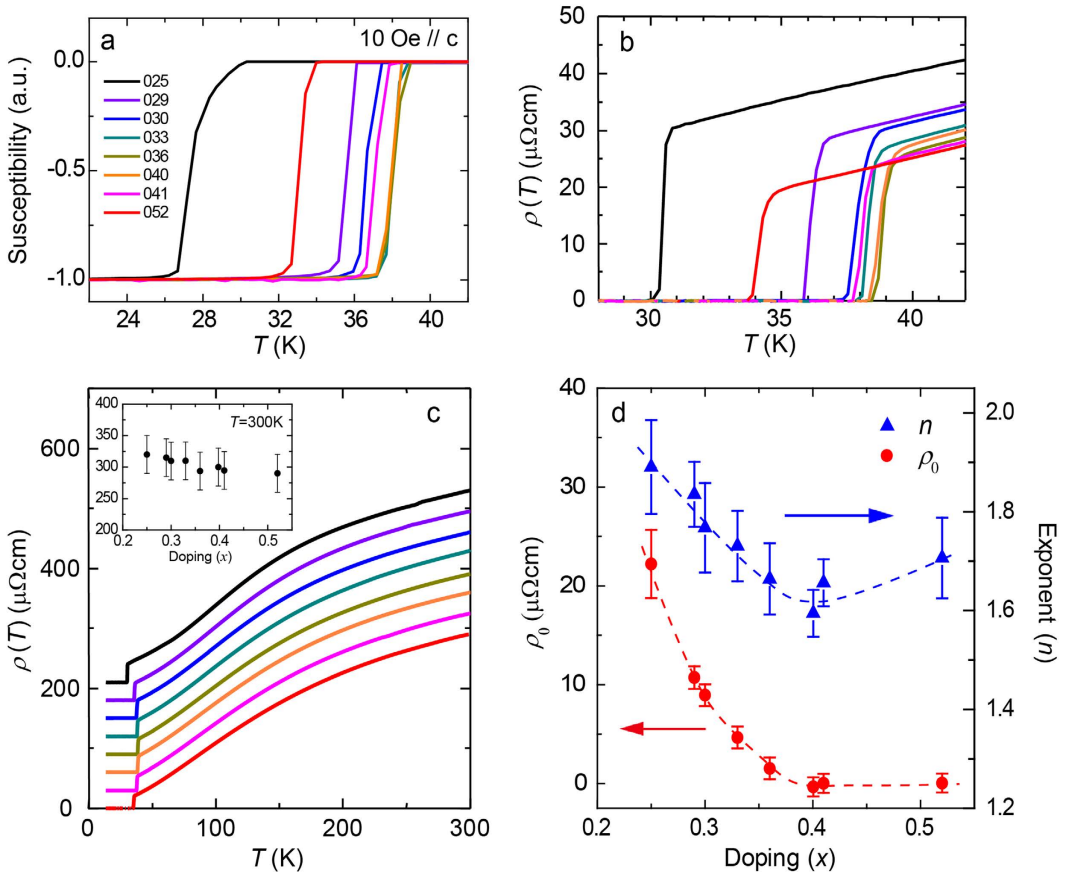

Figure 1. (**a**) Temperature dependence of the magnetic susceptibility of $Ba_{1-x}K_xFe_2As_2$ ($x = 0.25$–0.52). (**b,c**) Temperature dependence of the in-plane resistivity, $\rho(T)$, for the temperature range of 28 K to 42 K and 0 K to 300 K, respectively, with the same color cord used in (**a**). In (**c**), 30 μΩcm offset is applied for every doping increment and x dependence of room temperature resistivity, ρ(300 K), is shown in the inset. (**d**) Residual resistivity ρ_0 and exponent n extracted from $\rho(T)$ of the low temperature region by using a power-law fitting, $\rho(T) = \rho_0 + AT^n$.

associated with a peak at the finite magnetic field (H) appearing in the magnetization hysteresis loop (MHL). Thus, the study of the SMP effect is of great interest, from both academic and technological points of view.

So far, systematic doping (x) dependent studies of the $Ba(Fe_{1-x}Co_x)_2As_2$ and $BaFe_2(As_{1-x}P_x)_2$ single crystals have been reported[26–29]. It has been shown that a doping dependence of SMP and J_c are observed and the J_c tends to be high at particular doping concentrations. As for the source of pinning, various mechanism have been proposed, including domain boundary[26,30,31], compositional disorder[21,29], *etc.*, as shall be discussed later. Still, a consensus has not been reached so far. Similarly, $Ba_{1-x}K_xFe_2As_2$, the highest T_c and H_{c2} material among the 122-type superconductors[32,33], is also known to show SMP[20,22]. However, to the best of our knowledge, there has been no systematic study on the x-dependence of J_c in spite of its highest potential as a material for future applications. In this work, we report the systematic evolution of the vortex pinning behavior and J_c in the $Ba_{1-x}K_xFe_2As_2$ single crystals ranging from under- ($x = 0.25$) to over-doped ($x = 0.52$) compositions. We established a detailed x - J_c phase diagram, which is characterized by a spike-like peak at the slightly under-doped composition around $x \sim 0.30$. The behavior contrasts with the moderate dome-like x-dependence of the T_c with a broad maximum at $x \sim 0.3$ to 0.5. High J_c is apparently related to existence of the SMP which disappears at optimal- and over-doping composition. Possible mechanisms to account for the origin of the enhanced J_c will be discussed.

Results

Figure 1(a) shows the temperature (T)-dependence of the magnetic susceptibility (χ) for the $Ba_{1-x}K_xFe_2As_2$ single crystal samples measured under zero-field-cooling (ZFC) conditions with $H = 10$ Oe applied along the c-axis. (For a better comparison, the data are normalized by the magnitude at 5 K). The superconducting transition is sharp with $\Delta T_c < 0.5$ K except for $x = 0.25$, indicative of good sample quality. With increasing x, T_c increases from 27.5 K for $x = 0.25$ to 38.5 K for $x = 0.36$, then gradually decreases with further doping, down to 33 K for $x = 0.52$. We also performed the in-plane resistivity (ρ) measurements on these samples. The results are plotted in Fig. 1(b) ($28\,K \leq T \leq 42\,K$) and (c) ($0\,K \leq T \leq 300\,K$), respectively. We used the same color code as in Fig. 1(a). In Fig. 1(b), the superconducting transition of $Ba_{1-x}K_xFe_2As_2$ is very sharp ($\Delta T_c < 0.5$ K) and shows a x-dependence. T_c's defined as the zero resistance T's are in good agreement with those defined by χ, which exhibits a dome-like shape with the broad maximum spanning from $x \sim 0.3$ to 0.5.

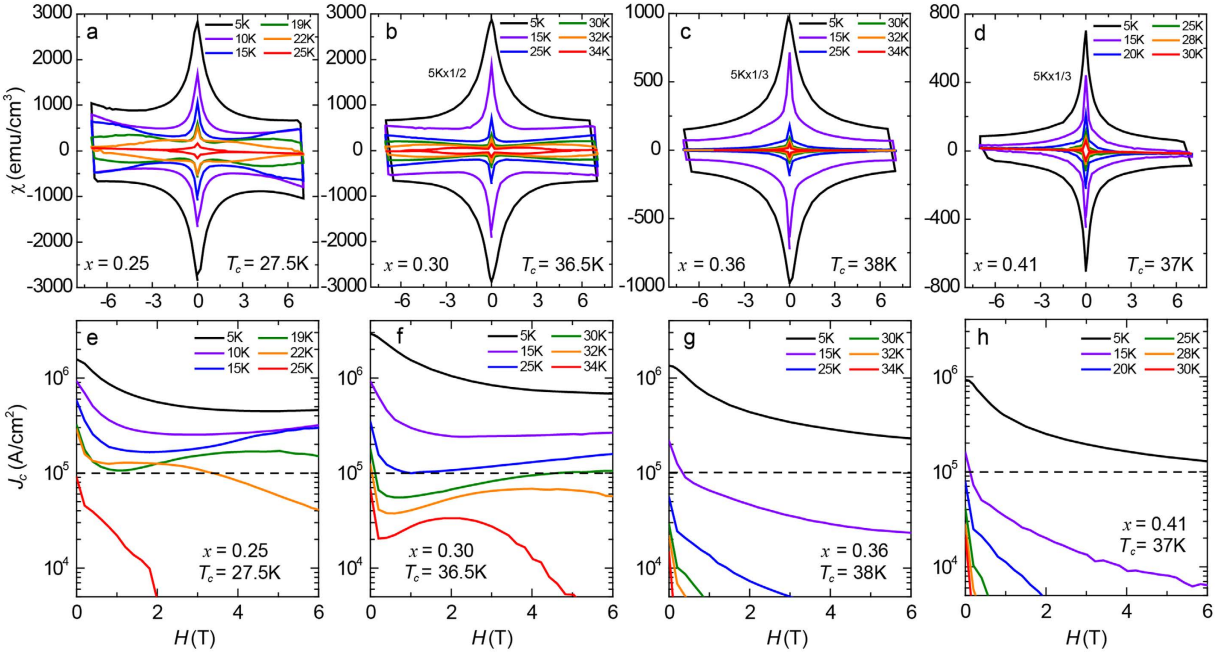

Figure 2. (**a–d**) Magnetization hysteresis loops (MHL) of $Ba_{1-x}K_xFe_2As_2$ with $x = 0.25$, 0.30, 0.36, and 0.41 measured at several temperatures. (**e,f**) Magnetic field and temperature dependence of the critical current density J_c determined by the Bean model from the MHL shown in (**a–d**), respectively. Dashed horizontal lines indicate the practical-level of $J_c = 10^5$ A/cm^2.

In Fig. 1(c), each ρ curve is shifted by 30 μΩcm to avoid an overlap. In the inset, the absolute value of ρ at 300 K, ρ(300 K), is plotted, which shows gradual decrease from 320 μΩcm ($x = 0.25$) to 290 μΩcm ($x = 0.52$). The overall shape of $\rho(T)$ is similar with each other, which shows the saturating behavior at the high T region, in other words, S-shaped T-dependence. For $x = 0.25$, anomaly in ρ is observed at around 65 K due to the anti-ferromagnetic/orthorhombic phase transition. In the low-T region, $\rho(T)$s are well fitted by a power-law function, $\rho(T) = \rho_0 + AT^n$ (the details of fitting procedure are described in Method section). The estimated residual resistivity ρ_0 and exponent n are shown in Fig. 1(d), which will be discussed later.

Figure 2(a–d) show typical MHLs measured at various T with H along the c axis. Each sample represents under-doped ($x = 0.25$, $T_c = 27.5$ K), slightly under-doped ($x = 0.30$, $T_c = 36.5$ K), optimally doped ($x = 0.36$, $T_c = 38$ K), and slightly over-doped ($x = 0.41$, $T_c = 37$ K) concentration, respectively. Qualitatively, the overall features measured at $T = 5$ K are more or less similar to each other in that they are characterized by a sharp peak centered at $H = 0$ and almost symmetric shapes with respect to H. The latter property indicates the dominant contribution of bulk pinning instead of a surface barrier[34]. These behaviors are also seen in various Fe-based superconductors. The width of the irreversible magnetization ΔM tends to shrink with increasing x. Moreover, at higher temperatures ($T > 15$ K), for $x = 0.25$ and 0.30, M increases with H after the initial decrease in the low H region, indicative of the SMP. The broad peaks are evident above 19 K for $x = 0.25$ and 30 K for $x = 0.30$, respectively. The position of the SMP moves towards higher H as T decreases and eventually goes beyond the accessible field range, $H = 7$ T in the present case. In contrast, for $x = 0.36$ and 0.41, M decreases monotonically with H at all T.

To determine J_c from the MHLs, we employed the extended Bean model[35], $J_c = 20\Delta M/[w(1 - w/3l)]$, where w and l are the dimensions of the rectangular sample ($w < l$). Figure 2(e–h) show the H-dependent J_c corresponding to the compositions shown in Fig. 2(a–d). The dashed lines indicate $J_c = 10^5$ A/cm^2, which is a threshold value for practical applications. At $T = 5$ K, J_c is the order of 10^6 A/cm^2 at zero field, 1.6×10^6 A/cm^2 ($x = 0.25$), 3.0×10^6 A/cm^2 ($x = 0.30$), 1.4×10^6 A/cm^2 ($x = 0.36$), and 0.9×10^6 A/cm^2 ($x = 0.41$), respectively. Among the four samples, J_c is the highest at $x = 0.30$. This crystal is slightly under-doped in terms of T_c, since T_c of the $x = 0.30$ sample is 36.5 K, lower than the highest T_c of 38 K at $x = 0.36$. The result shows that the highest J_c composition does not match the highest T_c composition in $Ba_{1-x}K_xFe_2As_2$. With increasing H, J_c decreases monotonically, while keeping high values above 10^5 A/cm^2 up to $H = 6$ T, 4.6×10^5 A/cm^2 ($x = 0.25$), 6.8×10^5 A/cm^2 ($x = 0.30$), 2.3×10^5 A/cm^2 ($x = 0.36$), and 1.3×10^5 A/cm^2 ($x = 0.41$), respectively, indicating the high current-carrying ability of this system at low T.

At higher T, J_c of the $x = 0.25$ and 0.30 samples exhibit a non-monotonic H dependence reflecting the SMP effect. As a consequence, the $x = 0.30$ sample sustains J_c exceeding 10^5 A/cm^2 even at $T = 25$ K and $H = 6$ T, showing the possibility of high magnetic field applications with an operation temperature above 20 K even without introducing artificial pinning center. On the other hand, the optimal- ($x = 0.36$) and over-doped ($x = 0.41$) samples always exhibit a monotonic decrease of J_c with H, resulting in a much lower J_c under high H.

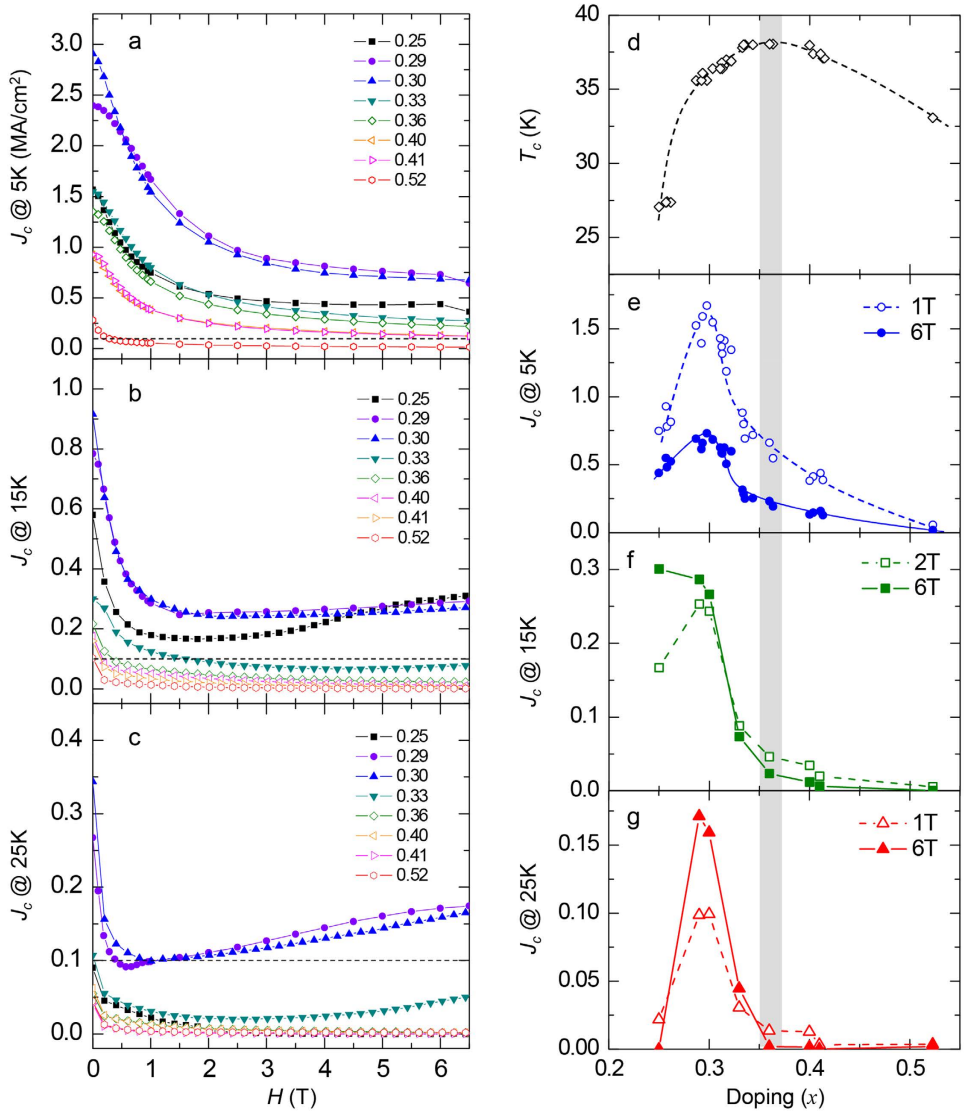

Figure 3. (**a–c**) Doping dependence of J_c as a function of magnetic field at 5 K, 15 K, and 25 K for $x = 0.25$, 0.29, 0.30, 0.33, 0.36, 0.40, 0.41, and 0.52. (**d**) Doping dependence of T_c for 26 samples. (**e**) J_c of the 26 samples at $T = 5$ K, $H = 1$ and 6 T. (**f,g**) Doping dependence of J_c at $T = 15$ and 25 K, respectively, with $H = 1$, 2 and 6 T extracted from (**b,c**). The shaded region in panels (**d–g**) indicates the optimal doping region, $x \sim 0.36$, showing maximum $T_c \sim 38.5$ K.

For a more detailed comparison, H-dependence of J_c for various x's ($x = 0.25$, 0.29, 0.30, 0.33, 0.36, 0.40, 0.41, 0.52) at 5 K, 15 K and 25 K are plotted in Fig. 3(a–c). For each T, J_c changes more than tenfold with changing x. At $T = 5$ K (Fig. 3(a)), crystals with $x = 0.29$ and 0.30 possess the highest J_c among all compositions. On the other hand, J_c rapidly decreases either with increasing or decreasing x. The resultant x-dependence is shown in Fig. 3(e), in which the J_c values at $H = 1$ and 6 T for 26 samples are plotted. A peak in J_c is observed around $x = 0.30$. The peak is sharp with its full width half maximum as small as 0.08. Therefore, the J_c-x phase diagram turns out to be very different from the T_c-x phase diagram which is shown in Fig. 3(d). First, the peak position is $x = 0.30$ for the former, while $x = 0.36$ for the latter. Second, J_c shows salient x-dependence, while T_c changes mildly with x.

At 15 K (Fig. 3(b)), non-monotonic H-dependence is seen for $x = 0.25$, $x = 0.29$, and $x = 0.30$. For these samples, J_c first decreases with H, then increases at high H. This behavior reflects the SMP observed in the MHL. In detail, the minimum J_c value of $x = 0.25$ at $H = 1.8$ T is smaller than that of $x = 0.29$ and 0.30 at $H = 1.5$ T and 2.2 T, respectively. On the contrary, the enhancement of J_c at high field is more prominent for $x = 0.25$ than that of $x = 0.29$ and 0.30, presumably because of the strong SMP effect of $x = 0.25$. Consequently, for the $H = 6$ T result shown in Fig. 3(f), the $x = 0.25$ sample exhibits the highest J_c, which is due to the steep increase of J_c with field. Meanwhile, as x increases above 0.33, J_c at $H = 0$ becomes smaller with x and decreases monotonically with H (Fig. 3(b)). As a result, J_c remains low (typically below 10^5 A/cm^2) in the entire H-region.

At 25 K (Fig. 3(c)), with disappearance of the SMP, J_c becomes significantly lower for $x = 0.25$ compared to $x = 0.29$ and $x = 0.30$. This is because the measurement T is close to T_c of the $x = 0.25$ sample ($T_c = 27.5$ K). For

$x = 0.29$ and 0.30, non-monotonic H-dependence persists and J_c's above 10^5 A/cm^2 are recorded up to $H = 6$ T except for the small H range around 0.5 T and 1 T, respectively. On the other hand, for $x = 0.33$ and above, J_c decreases down to the 10^4 A/cm^2 range, although they possess T_c much higher than the measurement T.

Discussion

As shown in Fig. 3(d–g), J_c and T_c of the $Ba_{1-x}K_xFe_2As_2$ single crystal samples show contrasting x-dependence. A distinct x-dependence of J_c and T_c is also reported for the $Ba(Fe_{1-x}Co_x)_2As_2$ and $BaFe_2(As_{1-x}P_x)_2$ single crystals[26–29]. In both cases, J_c exhibits marked x-dependence with a peak near the left end of the superconducting dome (under-doped region), while T_c gradually changes with x. Based on the $Ba(Fe_{1-x}Co_x)_2As_2$ results, R. Prozorov *et al.*[26] ascribed the characteristic J_c behavior to intrinsic pinning on the structural domains in the orthorhombic phase, which neighbors the superconducting phase on the under-doped side. On the other hand, based on the $BaFe_2(As_{1-x}P_x)_2$ single crystal results, S. Demirdiş *et al.*[29] and L. Fang *et al.*[28] proposed that the inhomogeneity in dopant distribution causes a spatial fluctuation of the superconducting condensation energy (δT_c pinning) and/or the mean free path (δl pinning)[36]. To our knowledge, most of the precedent MHL studies take the latter stance.

Existing phase diagrams of the $Ba_{1-x}K_xFe_2As_2$ system[37,38] show that the orthorhombic phase disappears between $x = 0.25$ and 0.30, which approximately matches with the composition where the enhancement of J_c is found. In this regard, the present results are compatible with the idea that the orthorhombic structural domains are the main source of vortex pinning. On the other hand, comparing Fig. 3(d,e), one notices that the high J_c is realized where the x-dependence of T_c (defined by dT_c/dx) is large. In such a situation, small compositional inhomogeneity results in large local variation in T_c, yielding δT_c pinning. In addition, the possible role of δl pinning to the enhanced J_c is suggested from the x-dependence of the residual resistivity ρ_0. In Fig. 1(d), exponent n decreases gradually with x from ~1.9 at $x = 0.25$ to ~1.6 at $x = 0.40$, then slightly increases to ~1.7 at $x = 0.52$. This result indicates that the T-linear contribution becomes large at around optimal x. However, the feature is not significant compared to $BaFe_2(As_{1-x}P_x)_2$ case[39] which shows certain variation in n from 2 to 1. On the other hand, ρ_0 rapidly decreases by more than twenty times from $x = 0.25$ to $x = 0.40$. In this doping range, carrier density is considered to evolve moderately, since the small change in the magnitude of ρ(300 K) as well as the small variation of n, $\sim 1.6 < n < \sim 1.9$, are observed. (see inset of Fig. 1(c)) Thus, it is natural to assume that the change in ρ_0 comes from the change in the mean free path (l) of the carriers, not due to the change in the carrier number[40]. From the same point of view, the x-dependence of ρ_0 in Fig. 1(d) reflects the x-dependence of l, which indicates that the δl pinning should be stronger in the under-doped samples, while it becomes weaker in the optimal- to over-doped samples. This tendency consistently explains the observed J_c behavior. Meanwhile, we should not rule out another possibility that some novel features such as quantum criticality and/or anti-ferromagnetic/orbital fluctuations are correlated with the origin of strong flux pinning of this system.

In any case, the present results clearly demonstrate that intra-grain J_c of the $Ba_{1-x}K_xFe_2As_2$ system takes the largest value at $x = 0.30$, which is different from the composition $x = 0.40$, commonly employed for fabricating PIT wires[12]. Although the real wires are composed of polycrystalline samples and their J_c's are affected by the inter-grain connectivity, as well as by the presence of pinning centers introduced either intentionally or accidentally, the present results suggest that J_c of PIT wires can be further increased by tuning the composition towards the lower doping side. This highlights the importance of fine chemical tuning for establishing and broadening the application potential of the $Ba_{1-x}K_xFe_2As_2$ superconductor.

Methods

The $Ba_{1-x}K_xFe_2As_2$ single crystals with doping concentration $x = 0.25$–0.52 were grown by the KAs self-flux method using a stainless-steel container, following the method depicted in ref. 41. The doping concentration of the grown crystals was successfully controlled by tuning the mixing ratio of Ba and Fe in the starting compositions. In total, ten batches of $Ba_{1-x}K_xFe_2As_2$ single crystals (two batches for $x \sim 0.25$, two batches for $x \sim 0.3$, two batches for $x \sim 0.33$, one batch for $x \sim 0.36$, two batches for $x \sim 0.4$, and one batch for $x \sim 0.5$, respectively) were grown for this study in order to check the reproducibility carefully. The compositions of the single crystals were confirmed by energy-dispersive X-ray (EDX) analysis and X-ray diffraction using Cu Kα radiation. The c-axis lengths determined by the X-ray diffraction were consistent with the compositions determined by EDX. The samples were cut into rectangular shapes with typical dimensions of 1 mm (length) × 0.8 mm (width) × 0.02 mm (thickness) for the magnetization and resistivity measurements. The T- and H- dependence of the magnetization were measured using a magnetic property measurement system (MPMS, Quantum Design). The resistivity measurements were carried out by a standard four probe method using a physical property measurement system (PPMS, Quantum Design). The data are reproducible and independent of the sample batch. We therefore believe that the present results represent intrinsic property of $Ba_{1-x}K_xFe_2As_2$ system. We fitted the $\rho(T)$ data using a power law function, $\rho(T) = \rho_0 + AT^n$, in the T range, $T_c < T < T_{up}$. The upper bound temperature (T_{up}) of fitting for each sample is taken well below the inflection point of S-shaped $\rho(T)$ in order to avoid underestimation of exponent n. Since the inflection point shifts from $T \sim 95$ K to $T \sim 80$ K as x increases from $x = 0.25$ to $x = 0.52$[42], T_{up} also gradually decreases from 80 K to 53 K.

References

1. Kamihara, Y. *et al.* Iron-Based Layered Superconductor $La(O_{1-x}F_x)FeAs$ ($x = 0.05-0.12$) with $T_c = 26$ K. *J. Am. Chem. Soc.* **130,** 3296 (2008).
2. Ren, Z. A. *et al.* Superconductivity at 55 K in iron-based F-doped layered quaternary compound $Sm[O_{1-x}F_x]FeAs$. *Chin. Phys. Lett.* **25,** 2215 (2008).
3. Senatore, C. *et al.* Upper critical fields well above 100 T for the superconductor $SmFeAsO_{0.85}F_{0.15}$ with $T_c = 46$ K. *Phys. Rev. B* **78,** 054514 (2008).

4. Jaroszynski, J. *et al.* Upper critical fields and thermally-activated transport of $NdFeAsO_{0.7}F_{0.3}$ single crystal. *Phys. Rev. B* **78,** 174523 (2008).
5. Yuan, H. Q. *et al.* Nearly isotropic superconductivity in $(Ba,K)Fe_2As_2$. *Nature (London)* **457,** 565 (2009).
6. Altarawneh, M. M. *et al.* Determination of anisotropic H_{c2} up to 60 T in $Ba_{0.55}K_{0.45}Fe_2As_2$ single crystals *Phys. Rev. B* **78,** 220505 (2008).
7. Katase, T. *et al.* Advantageous grain boundaries in iron pnictide superconductors. *Nat. Commun.* **2,** 409 (2011).
8. Weiss, J. D. *et al.* High intergrain critical current density in fine-grain $(Ba_{0.6}K_{0.4})Fe_2As_2$ wires and bulks. *Nature Mater.* **11,** 682 (2012)
9. Haindl, S. *et al.* Thin film growth of Fe-based superconductors: from fundamental properties to functional devices. A comparative review. *Rep. Prog. Phys.* **77,** 046502 (2014).
10. Ma, Y. *et al.* Progress in wire fabrication of iron-based superconductors. *Supercond. Sci. Technol.* **25,** 113001 (2012).
11. Sato, H. *et al.* High critical-current density with less anisotropy in $BaFe_2(As,P)_2$ epitaxial thin films: Effect of intentionally grown c-axis vortex-pinning centers. *Appl. Phys. Lett.* **104,** 182603 (2014).
12. Gao, Z. *et al.* High transport J_c in magnetic fields up to 28 T of stainless steel/Ag double sheathed Ba122 tapes fabricated by scalable rolling process. *Supercond. Sci. Technol.* **28,** 012001 (2015).
13. Zhang, X. *et al.* Realization of practical level current densities in $Sr_{0.6}K_{0.4}Fe_2As_2$ tape conductors for high-field applications. *Appl. Phys. Lett.* **104,** 202601 (2014).
14. Nakajima, Y. *et al.* Enhancement of critical current density in Co-doped $BaFe_2As_2$ with columnar defects introduced by heavy-ion irradiation. *Phys. Rev. B* **80,** 012510 (2009).
15. Fang, L. *et al.* High, magnetic field independent critical currents in $(Ba,K)Fe_2As_2$ crystals. *Appl. Phys. Lett.* **101,** 012601 (2012).
16. Fang, L. *et al.* Huge critical current density and tailored superconducting anisotropy in $SmFeAsO_{0.8}F_{0.15}$ by low-density columnar-defect incorporation. *Nature Commun.* **4,** 2655 (2013).
17. Tarantini, C. *et al.* Strong vortex pinning in Co-doped single crystal thin films. *Appl. Phys. Lett.* **96,** 142510 (2010).
18. Zhang, Y. *et al.* Self-assembled oxide nanopillars in epitaxial $BaFe_2As_2$ thin films for vortex pinning. *Appl. Phys. Lett.* **98,** 042509 (2011).
19. Prozorov, R. *et al.* Vortex phase diagram of $Ba(Fe_{0.93}Co_{0.07})_2As_2$ single crystals. *Phys. Rev. B* **78,** 224506 (2008).
20. Yang, H. *et al.* Fishtail effect and the vortex phase diagram of single crystal $Ba_{0.6}K_{0.4}Fe_2As_2$. *Appl. Phys. Lett.* **93,** 142506 (2008).
21. Yamamoto, A. *et al.* Small anisotropy, weak thermal fluctuations, and high field superconductivity in Co-doped iron pnictide. *Appl. Phys. Lett.* **94,** 062511 (2009).
22. Sun, D. L. *et al.* Comparative study of upper critical field H_{c2} and second magnetization peak H_{sp} in hole- and electron-doped $BaFe_2As_2$ superconductor. *Phys. Rev. B* **80,** 144515 (2009).
23. Yadav, C. S. *et al.* Upper critical field, lower critical field and critical current density of $FeTe_{0.60}Se_{0.40}$ single crystals. *New J. Phys.* **11,** 103046 (2009).
24. Van der Beek, C. J. *et al.* Flux pinning in $PrFeAsO_{0.9}$ and $NdFeAsO_{0.9}F_{0.1}$ superconducting crystals. *Phys. Rev. B* **81,** 174517 (2010).
25. Pramanik, A. K. *et al.* Fishtail effect and vortex dynamics in LiFeAs single crystals. *Phys. Rev. B* **83,** 094502 (2011).
26. Prozorov, R. *et al.* Intrinsic pinning on structural domains in underdoped single crystals of $Ba(Fe_{1-x}Co_x)_2As_2$. *Phys. Rev. B* **80,** 174517 (2009).
27. Shen, B. *et al.* Flux dynamics and vortex phase diagram in $Ba(Fe_{1-x}Co_x)_2As_2$ single crystals revealed by magnetization and its relaxation. *Phys. Rev. B* **81,** 014503 (2010).
28. Fang, L. *et al.* Doping- and irradiation-controlled pinning of vortices in $BaFe_2(As_1-_xP_x)_2$ single crystals. *Phys. Rev. B* **84,** 140504(R) (2011).
29. Demirdiş, S. *et al.* Disorder, critical currents, and vortex pinning energies in isovalently substituted $BaFe_2(As_{1-x}P_x)_2$. *Phys. Rev. B* **87,** 094506 (2013).
30. Kalisky, B. *et al.* Behavior of vortices near twin boundaries in underdoped $Ba(Fe_{1-x}Co_x)_2As_2$. *Phys. Rev. B* **83,** 064511 (2011).
31. Yang, H. *et al.* Vortex images on $Ba_{1-x}K_xFe_2As_2$ observed directly by magnetic force microscopy. *Phys. Rev. B* **85,** 014524 (2012).
32. Rotter, M. *et al.* Superconductivity at 38 K in the Iron Arsenide $(Ba_{1-x}K_x)Fe_2As_2$. *Phys. Rev. Lett.* **101,** 107006 (2008).
33. Tarantini, C. *et al.* Significant enhancement of upper critical fields by doping and strain in iron-based superconductors. *Phys. Rev. B* **84,** 184522 (2011).
34. Bean, C. P. *et al.* Surface Barrier in Type-II Superconductors. *Phys. Rev. Lett.* **12,** 14 (1964).
35. Bean, C. P. Magnetization of Hard Superconductors. *Phys. Rev. Lett.* **8,** 250 (1962).
36. Blatter, G. *et al.* Vortices in high-temperature superconductors. *Rev. Mod. Phys.* **66,** 1125 (1994).
37. M. Rotter, *et al.* Superconductivity and Crystal Structures of $(Ba_{1-x}K_x)Fe_2As_2$ ($x = 0$–1). *Angew. Chem., Int. Ed* **47,** 7949 (2008).
38. Avci, S. *et al.* Phase diagram of $Ba_{1-x}K_xFe_2As_2$. *Phys. Rev. B* **85,** 184507 (2012).
39. Kasahara, S. *et al.* Evolution from non-Fermi- to Fermi-liquid transport via isovalent doping in $BaFe_0(As_{1-x}P_x)_2$ superconductors. *Phys. Rev. B* **81,** 184519 (2010)
40. Consistent results showing $1/\tau_0 \sim \rho_0$ (τ_0: mean free time) have been reported in the optical study on $Ba(Fe_{1-x}Cox)_2As_2$ [M. Nakajima *et al.* Phys. Rev. B **81**, 104528 (2010)] and $LiFe_{1-x}Co_xAs$ [Y. M. Dai *et al.* Phys. Rev. X **5**, 031035 (2015)].
41. Kihou, K. *et al.* Single Crystal Growth and Characterization of the Iron-Based Superconductor KFe_2As_2 Synthesized by KAs Flux Method. *J. Phys. Soc. Jpn.* **79,** 124713 (2010).
42. Liu, Y. *et al.* Comprehensive scenario for single-crystal growth and doping dependence of resistivity and anisotropic upper critical fields in $(Ba_{1-x}K_x)Fe_2As_2$ ($0.22 \leq x \leq 1$). *Phys. Rev. B* **89,** 134504 (2014).

Acknowledgements

This work was supported by the Austrian Science Fund (FWF): P22837-N20, the European-Japanese collaborative project SUPER-IRON (No. 283204), SICORP of the Japan Science and Technology Agency (JST), and the Sasakawa Scientific Research Grant from The Japan Science Society. D.S. thanks the support from the Japan Society for the Promotion of Science (JSPS).

Author Contributions

D.S., S.I., A.I. and H.E. coordinated and designed the experiments. D.S., S.I. and M.N. grew the single crystals. D.S. and S.I. performed all the measurements and carried out analysis. J.S. and M.E. provide advice and consultation. D.S, S.I. and H.E. contributed to writing the manuscript. All authors discussed the result and commented on the manuscript.

Additional Information

Competing financial interests: The authors declare no competing financial interests.

How to cite this article: Song, D. *et al.* Distinct doping dependence of critical temperature and critical current density in $Ba_{1-x}K_xFe_2As_2$ superconductor. *Sci. Rep.* **6**, 26671; doi: 10.1038/srep26671 (2016).